Deep subwavelength optical imaging using correlated nano-torches

Yuecheng Shen, Lihong V. Wang, and Jung-Tsung Shen

Citation: Applied Physics Letters **103**, 201119 (2013); doi: 10.1063/1.4832070

View online: http://dx.doi.org/10.1063/1.4832070

View Table of Contents: http://scitation.aip.org/content/aip/journal/apl/103/20?ver=pdfcov

Published by the AIP Publishing

Deep subwavelength optical imaging using correlated nano-torches

Yuecheng Shen,[1,a)] Lihong V. Wang,[2] and Jung-Tsung Shen[1,b)]
[1]*Department of Electrical and Systems Engineering, Washington University in St. Louis, St. Louis, Missouri 63130, USA*
[2]*Department of Biomedical Engineering, Washington University in St. Louis, St. Louis, Missouri 63130, USA*

(Received 6 September 2013; accepted 4 November 2013; published online 15 November 2013)

The authors propose and numerically demonstrate an ultra-high resolution (wavelength/50∼40 nm at wavelength $\lambda = 2.08\,\mu$m), high-throughput (∼66%), and non-destructive optical lens with a large contrast-to-noise ratio, based on the notion of correlated nano-torches formed in a subwavelength metallic grating. The correlations between the torches also allow the determination of the complex refractive index of the sample. © *2013 AIP Publishing LLC*. [http://dx.doi.org/10.1063/1.4832070]

Deep subwavelength optical imaging, i.e., the capability to discern details much smaller than the wavelength of the illuminating light, will have a strong impact in the life science and in a broad range of next-generation scientific and industrial applications. State-of-the-art approaches to beat the diffraction limit in optical imaging include using (1) artificially engineered materials (e.g., superlens[1] and hyperlens[2]) and (2) fluorescent markers, such as photo-activated localization microscopy (PALM)[3] and stochastic optical reconstruction microscopy (STORM).[4] Despite demonstrated superior performance, the implementations of these sophisticated techniques face fundamental challenges,[5] including material attenuation and as yet unattainable fabrication finesse, or only work for a narrow class of samples.[6–8] Another approach to achieve deep subwavelength resolution is the near-field scanning optical microscopy (NSOM).[9,10] Still, NSOM suffers from low transmissivity of optical signals as the apertures are far smaller than the incident light wavelength. Here, we propose and numerically demonstrate an ultra-high resolution (wavelength/50), high-throughput (∼66%), and non-destructive optical lens with a large contrast-to-noise ratio, based on the notion of correlated nano-torches formed in a subwavelength metallic grating. The correlations between the nano-torches also allow the determination of the complex refractive index of the sample.

In practice, even with the enormous advances brought about by electron and scanning probe microscopy, about 80% of all microscopy investigations in the life sciences are still carried out optically.[11] It is thus highly desirable to develop a robust optical imaging technique that overcomes at least some of the limitations in the current approaches. This article proposes a conceptually ultra-high resolution, high-throughput, and non-destructive optical lens based on artificially engineered materials for optical imaging that beats the resolution limit of conventional optical instruments and of the recently demonstrated superlens and hyperlens. The key enabling mechanism to achieve ultra-high resolution is to create an array of correlated nano-torches to light up the surrounding sample: each nano-torch has a linear dimension that is far smaller than the wavelength and contains strong evanescent fields that greatly enhance the light-matter interactions. In such a mechanism, the resolution is primarily determined by the size of the nano-torch rather than the wavelength of the illuminating light. Moreover, the brightness of each nano-torch depends on the light-matter interactions occurred at its neighboring torches. The correlations between the torches enable the differentiation of contributions from the scattering and absorption of the signal, thereby allowing the determination for the *complex* refractive index of the sample. The mechanism is also potentially scalable for different illuminating wavelengths as long as the criteria for correlated nano-torches are satisfied.

The simplest realization of the nano-torches-lens is a one-dimensional subwavelength metallic grating (Fig. 1). To demonstrate the superior performance, we show numerically that the lens can achieve a resolution of $\lambda/50$ (∼40 nm at wavelength $\lambda = 2.08\,\mu$m) and has an extraordinarily large signal throughput, even in the presence of material attenuation. We further show that near-field information can be encoded into propagating waves by coupling the nano-torches-lens to a passive waveguide. Owing to the large electric field enhancement, the lens provides a large contrast-to-noise ratio (CNR) and thus is robust to external noises.

The nano-torches-lens is made of a metallic thin film with periodic cut-through slits, which can be either filled with transparent dielectric materials or left unfilled. The slit width a and the grating periodicity d are in the subwavelength regime, i.e., $a < d < \lambda$. It has been shown both theoretically[12] and experimentally[13] that the lens exhibits artificial dielectric behaviors and can be precisely mapped into a homogenous dielectric slab, showing a Fabry-Perot transmission spectrum. At resonant frequencies, the lens permits a large signal throughput for an incoming TE wave (i.e., transverse electric field pointing in the x-direction), which could increase the signal-to-noise ratio (SNR) when noises have fixed power levels as limited by the detection system. The extraordinary transmission is due to the subwavelength periodic structure and cannot be achieved by using only a single slit. Moreover, the electric fields in the slits are greatly enhanced (the enhancement factor is d/a for perfect electric conductor[12]), and strong evanescent torches are formed at both ends of each slit, which enhance the light-matter interactions (Fig. 1). In this article, we show that the lateral resolution of the image is determined by the torch size, which can be one or two orders of magnitude smaller than the

[a)]Electronic mail: ycshen@ese.wustl.edu
[b)]Electronic mail: jushen@ese.wustl.edu

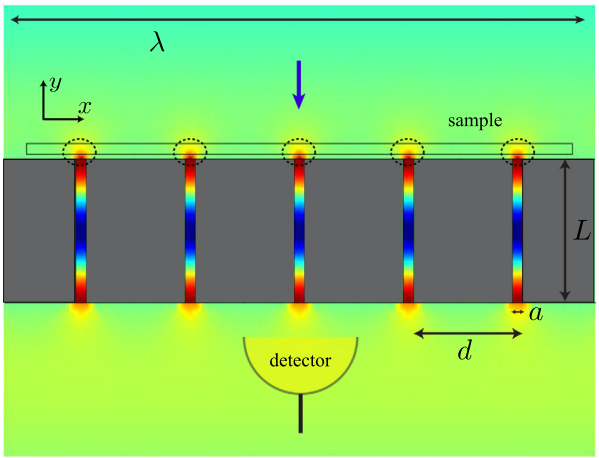

FIG. 1. Schematic of the nano-torches-lens. The dashed circles denote the bright nano-torches. The downward blue arrow indicates the direction of the incoming light. The background color indicates the x-component of the electric field profile for an incoming TE plane wave from simulation.

wavelength. The size of each torch in the x-direction is defined as the full width at half maximum (FWHM) of the electric field; numerically, it is found to be on the same order of the slit width.

To perform the imaging process, here we describe the general scheme as follows:

1. *System setup:* A sample is placed on the same side of the illuminating light beam to interact with the evanescent torches (Fig. 1). On the other side of the lens, a detector is placed in the proximity of one slit (detection slit) to measure from the slit the output optical flux (thus the field strength). One important feature of the nano-torches-lens is that the slit transmissions are coupled so that when one slit is covered by the sample, the field strengths in its neighboring slits are modified as well. Consequently, each measurement includes information about the local optical properties in all nano-torches at the same time.
2. *Data acquisition:* Consider a long sample with an unknown refractive index profile $n(x)$ which is to be determined. $n(x)$ is assumed to be real for now. The following procedure determines $n(x)$ over a continuous segment with length Nd, where N is an arbitrary positive integer. The refractive index of the sample beyond the segment is assumed to be n_b uniformly.
   (i) Select a step size δ, which also specifies the pixel size in the reconstructed image. The imaging resolution will be found to be $\max\{a, \delta\}$.
   (ii) Divide the segment into $N\Delta$ slices, where $\Delta = d/\delta$. Without losing generality, here we assume $\delta = a$, and the lens is designed such that d/a is an integer. The index of each slice is taken as uniform and is denoted by n_i, $i = 1, 2, \cdots, N\Delta$, from right to left.
   (iii) Start with the $i = 1$ slice covering the detection slit and record the measurement E_1. Note that the other slits are covered by the recurrent slices labeled by $i = 1 + \Delta, 1 + 2\Delta, \cdots, 1 + (N-1)\Delta$. The set of the slices is collectively denoted by S_1.
   (iv) Shift the sample by δ in the x-direction so that now the $i = 2$ slice covers the detection slit. Record the measurement E_2. Now the other slits are covered by the recurrent slices labeled by $i = 2 + \Delta, 2 + 2\Delta, \cdots, 2 + (N-1)\Delta$. The set of the slices is collectively denoted by S_2. S_1 and S_2 are exclusive. Fig. 2 depicts the configurations for the slices comprising a general set S_j.
   (v) Repeat the shift till $i = N\Delta$ slice covers the detection slit and record the measurement $E_{N\Delta}$. These $N\Delta$ measurements $\{E_1, E_2, \cdots, E_{N\Delta}\}$ can be partitioned into Δ groups, according to the slice set S_j, $j = 1, 2, \cdots, \Delta$. Each group contains N measurements.

To extract the global information of the sample, we develop a highly efficient and accurate inverse differential algorithm to reconstruct the image from the measurements as follows.

3. *Reconstruction algorithm:* All the measurements in the same group are coupled. To extract the information of $n(x)$, we envision the inhomogeneous sample being imaged is derived from a uniform material with index n_b and compare the differential between measurements. The total field differential introduced by the sample is a linear summation of the contributions from all slits, and each contribution is proportional to the local index variation at every slit. For example, the first measurement E_j in the j-th group is taken to have the following form:

$$E_j = E_b + (n_j - n_b)C_0E_{\text{inc}} + (n_{(j+\Delta)} - n_b)C_1E_{\text{inc}} + (n_{(j+2\Delta)} - n_b)C_2E_{\text{inc}} + \cdots, \quad (1)$$

where E_{inc} is the electric field of the incoming light, and E_b is the reference field for a uniform sample with index n_b, which can be obtained either numerically or experimentally. The dimensionless quantity C_i, $i = 0, 1, 2, \cdots$ describes the self- and mutual-couplings between the detection slit and its neighboring slits (Fig. 2). C_i's can be either positive or negative and can be numerically determined for specified index variation. Within the j-th

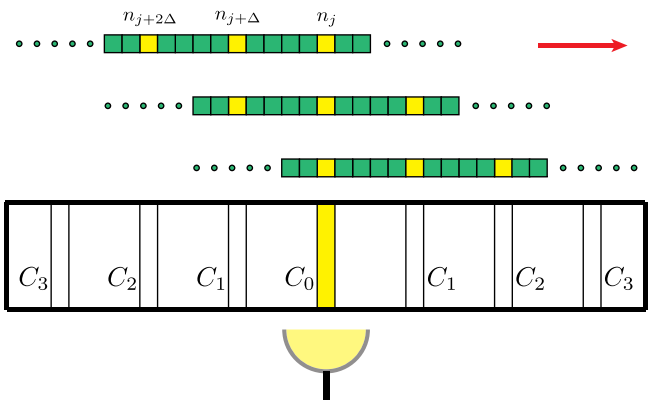

FIG. 2. Data acquisition process. Shown are three non-consecutive configurations of the slices (highlighted in yellow color) comprising a general set S_j. The measurements for all configurations for S_j form the j-th group. Coupling constants C_i's are labeled at corresponding slits. The red arrow indicates the shifting direction.

group, the N measurements can be recast into a compact matrix form

$$\begin{pmatrix} C_0 & C_1 & C_2 & \cdots & C_{N-1} \\ C_1 & C_0 & C_1 & \cdots & C_{N-2} \\ C_2 & C_1 & C_0 & \cdots & C_{N-3} \\ \vdots & \vdots & \vdots & \vdots & \vdots \\ C_{N-1} & C_{N-2} & C_{N-3} & \cdots & C_0 \end{pmatrix}_{N\times N} \begin{pmatrix} \Delta n_j \\ \Delta n_{(j+\Delta)} \\ \Delta n_{(j+2\Delta)} \\ \vdots \\ \Delta n_{(j+(N-1)\Delta)} \end{pmatrix}_{N\times 1} = \begin{pmatrix} \Delta\tilde{E}_j \\ \Delta\tilde{E}_{(j+\Delta)} \\ \Delta\tilde{E}_{(j+2\Delta)} \\ \vdots \\ \Delta\tilde{E}_{(j+(N-1)\Delta)} \end{pmatrix}_{N\times 1}, \quad (2)$$

where $\Delta\tilde{E}_j = (E_j - E_b)/E_{\text{inc}}$ is the normalized field differential and $\Delta n_j = n_j - n_b$ is the index variation of slice j. Repeating the process for all groups to solve for all Δn provides $n(x)$ for the entire segment being imaged. It is worth mentioning that a rescaling of all C_i's. does not change the contrast of the reconstructed image. Moreover, in practice, the nano-torches-lens can be designed such that only the first few C_i's. make contributions. Such an approach is validated by numerical simulations; it is numerically found that a good choice of n_b based upon the knowledge of the sample greatly increases the accuracy. The algorithm is also robust for a fairly wide range of n_b. One of the advantages of the differential algorithm is that as only the differential of the fields is used, ultra-high resolution can still be achieved even if fabrication imperfections are present in the grating.

Having introduced the general scheme, we now demonstrate the superior performance of the nano-torches-lens. Applying the reconstruction algorithm, Fig. 3(a) shows the reconstructed images of a 40 nm-thick sample containing a single defect ($n = 1.54893$, e.g., Barium crown glass, N-BAK1) in an otherwise uniform silica slab ($n = 1.43689$ (Ref. 14)). The lens is made of silver, which has an index $n_{\text{Ag}} = 0.99886 - 14.128i$ (Ref. 15) at wavelength $\lambda = 2.08\ \mu$m (e.g., HO:YAG laser). The grating with unfilled slits is designed so that $d = 400$ nm and $a = 40$ nm, and the thickness is $L = 662$ nm such that the grating is on resonance with the illuminating light. Numerically, the lens transmits 66% of light and reflects only 3% (the remainder dissipates). n_b is chosen to be the index of silica. The defects with different sizes $s = 60$ nm, 40 nm, 20 nm, and 10 nm, respectively, are imaged. The reconstructed images have FWHM 70 nm, 62 nm, 58 nm, and 53 nm, respectively. For even smaller defects, the FWHM is found numerically to approach the size of the light torch ($\sim a$), which gives the width of the point spread function (PSF) of the imaging system. That is, for features that are smaller than the slit width, their images are blurred to no less than the slit width. We note that the two kinks in the two larger samples and the two peaks in the two smaller samples are due to the strong evanescent electric field in the y-direction right at the corner of the slits; numerically, we found that they disappear when the sample is slightly translated away (say 10 nm) from the lens.

Next, we investigate the resolving power of the nano-torches-lens to distinguish a small distance g between two

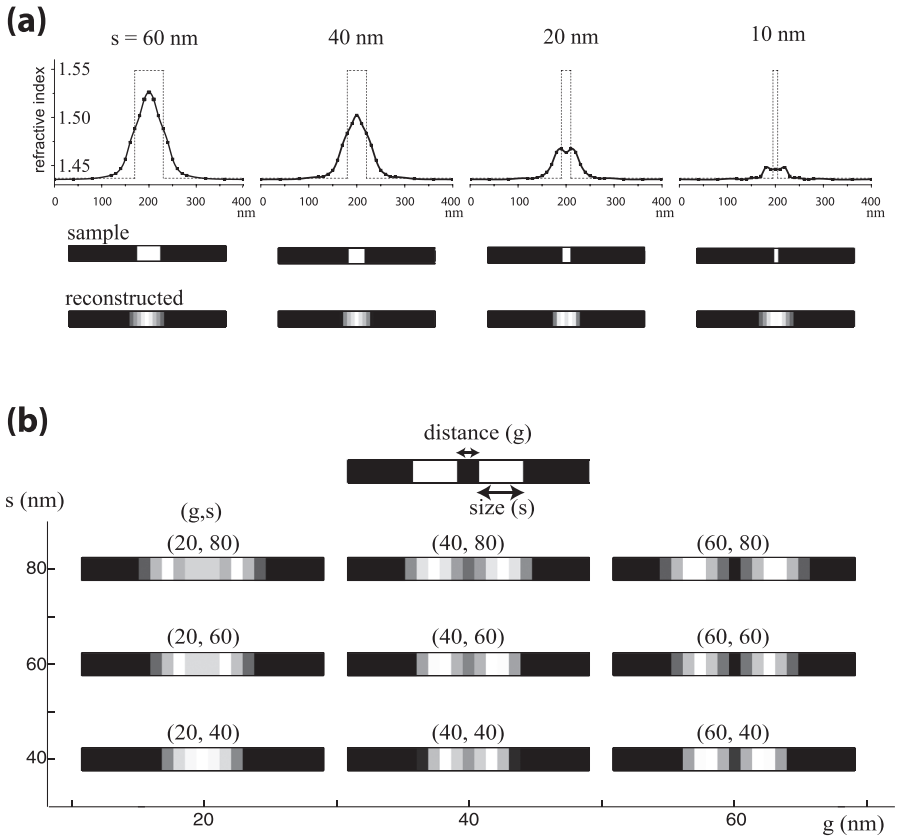

FIG. 3. Resolving power of the nano-torches-lens. (a) Reconstructed images of a small defect in an otherwise uniform silica. The dashed lines describe the sample index profile while the black dots connected by solid lines denote the reconstructed index profile. To aid the visualization, the sample and the reconstructed images are also plotted using the grey scale color map, with white and black colors indicating the maximum and minimum values, respectively, in each case. (b) Reconstructed images of two small defects in proximity, with varying size and separation.

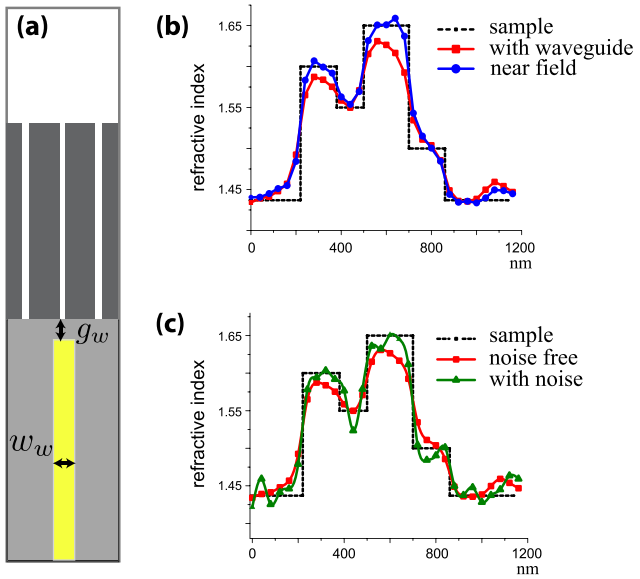

FIG. 4. Near-field perturbation and noises. (a) Schematic of a slab waveguide in the proximity of the detection slit. (b) Index profile of the sample (dashed line), the reconstructed index profile with (red squares) and without (blue dots) the waveguide. The thick lines in the reconstructed profiles are obtained by the spline interpolation method. (c) Index profile of the sample (dashed line) and of the reconstructed image with (green triangles) and without (red squares) noises.

small defects with size s each. The reconstructed images are shown in Fig. 3(b). The results indicate that when $g \geq 40\,\text{nm}$ $(=a)$, the two defects can always be distinguished regardless of their sizes. On the other hand, the results show that a very small distance ($g = 20\,\text{nm}$) between two large defects ($s = 80$, 60 nm) can be resolved by the lens. Such a case, from our algorithm, can be considered as complementary to the case wherein a small defect with size g is embedded in an otherwise homogenous material. The result does not violate the well known Abbe-Rayleigh criterion, which describes the resolving power between two point objects.

Till now, we assume that the detector placed in the near field does not perturb the measurements significantly. In practice, such a perturbation is unavoidable. Here we show that accurate image reconstruction is still possible in the presence of near-field perturbation. Consider a slab waveguide penetrating the light torch of the detection slit (Fig. 4(a)). The waveguide perturbs the strong evanescent field and excites propagating waves inside the waveguide, which can be propagated afar to the measurement end. Fig. 4(b) shows the reconstructed image for a 1.2 μm long sample, and both the reconstructed images with (red squares) and without (blue dots) the waveguide are in good agreement with the original index profile. The slab waveguide is made of silicon ($n = 3.44989$ (Ref. 14)), embedded in a silica substrate. The width of the slab waveguide is $w_w = 250$ nm, and the gap between the waveguide and the lens is $g_w = 210$ nm, determined through an optimization procedure: w_w is fixed so that only the first three coupling constants are significant, with $|C_1/C_0| = 0.67 > |C_2/C_0| = 0.29 \gg |C_3/C_0| = 0.03$; g_w is decided by maximizing $|C_0|$ so that the contrast in the image is as large as possible. Another important factor that degrades the performance of any imaging system is noise. Here we demonstrate the robustness of the nano-torches-lens against external local random noises by adding noises to the measurements. The intensity of random noises is represented by $0.2\% \times I \times C_{\text{Rand}}$, where I is the incident intensity and C_{Rand} is an equidistributed random number between $[-1,1]$. Fig. 4(c) shows the reconstructed image with (green triangles) and without (red squares) noises, assuming the waveguide is present.

In most biological tissues, due to light scattering and absorption, the optical property is described by a spatially varying complex refractive index: $\tilde{n}(x) = n(x) + i\kappa(x)$. The correlations between the slits allow us to determine $\tilde{n}(x)$ in one scanning using two detectors. In such a situation, when one slit is covered by a sample with a complex index, $n(x)$ and $\kappa(x)$ contribute independently to the total measured differential field (in general $n(x)$ and $\kappa(x)$ give rise to two different sets of coupling constants). By measuring at two neighboring slits (or in general, any two correlated slits), $\tilde{n}(x)$ can be determined by applying the reconstruction algorithm outlined above. Fig. 5 shows the reconstructed complex refractive index profile. Such a capability to reconstruct the complex index based on correlations is not possible in a single-slit scenario.

The nano-torches-lens enables a promising alternative modality to achieve ultra-high resolution in optical imaging. To accelerate the data acquisition process, simultaneous multi-channel detection can be employed, and, moreover, the sample may be shifted continuously and steadily while the detector is timed to take measurements at fixed time intervals. For samples with exceedingly large index contrast, the reconstruction algorithm can be generalized to include a nonlinear differential. More distinctively, the lens can be made to work over a wide frequency range from microwave to visible, by properly scaling down the dimensions of the

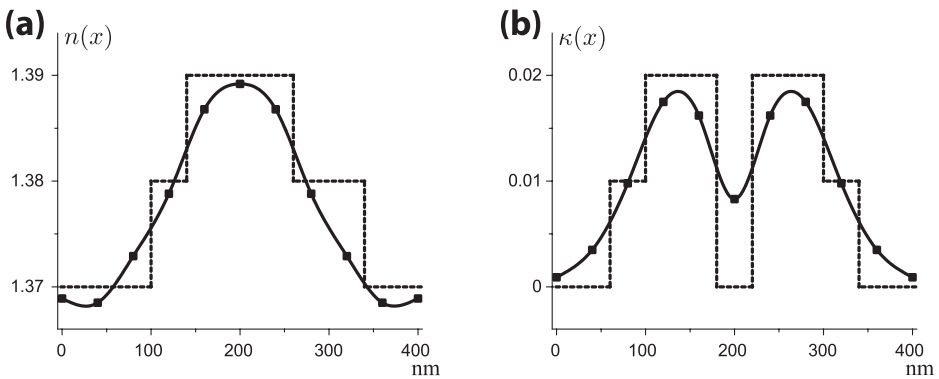

FIG. 5. Reconstruction of the complex refractive index. (a) The real part. The sample is denoted by the dashed line and the reconstructed image is denoted by black dots connected with a solid line. (b) The imaginary part.

grating. At visible light frequencies, the plasmonic effects become more important,[16] and the material attenuations and skin effects (fields penetrating into the metal) dilate the torches. Nonetheless, with narrower periodic slits, correlated torches that are orders-of-magnitude smaller than the wavelength can still be created, and relatively large signal throughput can be maintained. Such a scalability provides a unique opportunity to find broad applications. The reconstruction of a two-dimensional image can be obtained from a series of one-dimensional scanning, a process akin to the inverse Radon transformation in x-ray computed tomography (CT). These capabilities certainly will greatly extend the applicability of the nano-torches-lens. Finally, we comment on the current state of the art in plasmonic slits. Recently Verslegers *et al*. considered planar lens with plasmonic slits.[17,18] The periodic array case[17] makes use of the artificial dielectrics mechanism[12] and are designed to operate as far-field lenses to focus the incoming light, with a waist width much larger than the wavelength of the illumination, while the aperiodic array case[18] can achieve deep-subwavelength focusing only within the structure. In contrast, the lens described here achieves super-resolution by forming a periodic array of nano-torches in the near-field mode and a reconstruction algorithm; the range in the sample to be probed by the lens is limited by the longitudinal extension of the nano-torches in the *y*-direction. The resolving power decreases when the sample moves away from the nano-torches.

This work was supported by the National Science Foundation (ECCS-1254649).

[1]J. Pendry, Phys. Rev. Lett. **85**, 3966 (2000).
[2]Z. Jacob, L. Alekseyev, and E. Narimanov, *NanoScience + Engineering* (International Society for Optics and Photonics, 2007), p. 66380W.
[3]E. Betzig, G. Patterson, R. Sougrat, W. Lindwasser, S. Olenych, J. Bonifacino, M. Davidson, J. Lippincott-Schwartz, and H. Hess, Science **313**, 1642 (2006).
[4]M. Rust, M. Bates, and X. Zhuang, Nat. Methods **3**, 793 (2006).
[5]E. Rogers, J. Lindberg, T. Roy, S. Savo, J. Chad, M. Dennis, and N. Zheludev, Nat. Mater. **11**, 432 (2012).
[6]S. Hell, Nat. Biotechnol. **21**, 1347 (2003).
[7]B. Huang, W. Wang, M. Bates, and X. Zhuang, Science **319**, 810 (2008).
[8]S. Gazit, A. Szameit, Y. C. Eldar, and M. Segev, Opt. Express **17**, 23920 (2009).
[9]D. Pohl, W. Denk, and M. Lanz, Appl. Phys. Lett. **44**, 651 (1984).
[10]E. Betzig, A. Lewis, A. Harootunian, M. Isaacson, and E. Kratschmer, Biophys. J. **49**, 269 (1986).
[11]S. W. Hell, Science **316**, 1153 (2007).
[12]J. T. Shen, P. B. Catrysse, and S. Fan, Phys. Rev. Lett. **94**, 197401 (2005).
[13]A. Pimenov and A. Loidl, Phys. Rev. B **74**, 193102 (2006).
[14]M. Bass, C. DeCusatis, J. Enoch, V. Lakshminarayanan, G. Li, C. MacDonald, V. Mahajan, and E. Stryland, *Handbook of Optics: Optical Properties of Materials, Nonlinear Optics, Quantum Optics*, 3rd ed. (McGraw-Hill, 2009), Vol. IV.
[15]E. Palik, *Handbook of Optical Constants of Solids: Index* (Academic Press, 1998), Vol. 3.
[16]P. B. Catrysse, G. Veronis, H. Shin, J.-T. Shen, and S. Fan, Appl. Phys. Lett. **88**, 031101 (2006).
[17]L. Verslegers, P. B. Catrysse, Z. Yu, J. S. White, E. S. Barnard, M. L. Brongersma, and S. Fan, Nano Lett. **9**, 235 (2009).
[18]L. Verslegers, P. B. Catrysse, Z. Yu, and S. Fan, Phys. Rev. Lett. **103**, 033902 (2009).